The International Journal of Advanced Manufacturing Technology (2018) 97:2715–2729
https://doi.org/10.1007/s00170-018-2121-8

ORIGINAL ARTICLE

An experimental and theoretical analysis of surface generation in the ultra-precision grinding of hard and brittle materials

Shan Shan Chen[1,2] · Chi Fai Cheung[2] · Fei Hu Zhang[1]

Received: 5 November 2017 / Accepted: 6 May 2018 / Published online: 19 May 2018

Abstract

This paper presents an experimental and theoretical study of surface generation in the ultra-precision grinding of hard and brittle materials. The study takes into account the material properties, the relative vibration between the grinding wheel and the workpiece, the machining parameters and the phase shift of the grinding process. The Taguchi approach is employed to study the influence of machining parameters on the surface quality and shows that the feed speed and rotational speed of the workpiece are key factors. Experiments have been conducted to study individual variables, and the results further show that the feed rate and the cross-feed distance have a significant effect on surface generation. It is found that the spirals around the central area of the workpiece are the primary mechanism for surface generation, which originates from the synchronous relative tool-work vibration. The integral part of the ratio of the rotational speed of the grinding wheel to rotational speed of the workpiece determines the number of spirals and its fractional part controls the spiral geometry. A theoretical model for predicting the single spiral generation has been developed to explain the accumulation of the phase shift and the geometry. The changeable feed speed near the end of grinding is also modelled, revealing the approximate straight lines around one circle in the central region. The simulated results indicate that the theoretical models and the ground surfaces are in close agreement. The scallop-height model is developed to calculate the influence of phase shift on surface quality, and it is found that the phase shift near the medium value can effectively improve surface quality. Finally, a comparison of different surface generation mechanisms in grinding mould steel, tungsten carbide (WC) and reaction bonded silicon carbide (RB-SiC) is made. It is interesting to note that the Spanzipfel effect contributes to the surface generation not only on ductile materials such as mould steel but also on brittle materials such as WC and RB-SiC. The Spanzipfel effect is the most significant in grinding mould steel. For WC and RB-SiC, the ground surface contains both a ductile region and a brittle region in the form of micro-fractures.

Keywords Spiral · Phase shift · Spanzipfel · Surface generation mechanism · Ultra-precision grinding · Hard and brittle materials

1 Introduction

Ultra-precision grinding is widely applied to machine hard and brittle materials with high surface integrity and low surface roughness [1–4]. Reaction bonded silicon carbide (RB-SiC) ceramic has become the preferred mirror material for space telescopes due to its excellent mechanical properties, such as high hardness, high rigidity and chemical inertness [5–7]. However, it is a challenge to obtain a desirable surface finish in the grinding due to its low fracture toughness. Surface quality is the crucial indicator to evaluate the grinding performance, which results from the interaction of the tool and machined material. A high-quality surface finish significantly improves the functional performance of components, such as fatigue strength, frictional properties and life [8, 9]. Surface generation, as an important issue in the grinding process, is directly related to the surface quality and functional performance of the workpiece. This has attracted much research attention due to the ever-increasing requirements of precision components with good surface finish. However, the surface generation in ultra-precision grinding is affected by a multiplicity of variables

✉ Shan Shan Chen
shanshan.chen@connect.polyu.hk

[1] School of Mechatronics Engineering, Harbin Institute of Technology, Harbin 150001, China

[2] Partner State Key Laboratory of Ultraprecision Machining Technology, Department of Industrial and Systems Engineering, The Hong Kong Polytechnic University, Hung Hom, Kowloon, Hong Kong

involving the wheel geometry, abrasive distribution, material properties and grinding operation conditions. This is particularly true for the random nature of the cutting edges on the wheel which makes it difficult to study the process of surface generation and surface topography as compared with deterministic machining processes such as single-point diamond turning and milling.

Huang et al. [10] investigated the effect of rotational speed of the wheel on the ground surface quality in grinding silicon nitride through a series of experiments and found that the surface quality (ductile mode) is improved with increasing rotational speed of the wheel. However, for surface generation (brittle mode), it is insignificantly affected by the variations of the rotational speed of the wheel and the wheel spindle vibration caused by the wheel unbalance limits the improvement of the ground surface quality. Zhang et al. [11] investigated the different surface generation mechanisms both for WC/Co and RB-SiC and found that phase boundary cracking is the dominant mode, but for WC/Co, plastic deformation and grain dislodgement are the primary mechanisms governing the surface generation. Kwak [12] used the Taguchi parametric optimization approach to evaluate the effects of process parameters and grain size on geometric errors of the workpiece. It was found that the depth of cut is the dominant factor to determine the geometric error. Allor et al. [13] investigated the effects of abrasive sizes and concentration in grinding, and they found that the size of abrasive grain and the speed of grinding wheel are significant factors affecting the surface roughness. Oliveira et al. [14] studied dressing variables, such as dressing depth, dressing velocity and geometry of the dressing tool which can affect the surface topography generation of the grinding wheel. It was found that the wheel pattern produced by dressing can improve the machined surface roughness.

For theoretical analysis of surface generation in grinding, Ohbuchi and Obikawa [15] proposed a model of surface generation by considering the upheaval and residual volumetric material removal resulting from different grain shapes and cutting speeds. Agarwal and Rao [16] developed an analytical model to predict the surface roughness based on the statistical characteristics of the distribution of the abrasive grain and protrusion heights. Warnecke and Zitt [17] established a synthetic 3D model by considering the macro profile of the grinding wheel and micro-grain geometry combined with grinding kinematics to describe the process of the generation of surface topography. Cao et al. [18] established a model by combining the relative micro-vibration between the grinding tool and the workpiece with the micro-interacting behaviour of the active grains to determine the impact of the vibration amplitude, grit size and process parameters on surface generation in grinding. Actually, grinding marks caused by wheel vibration severely deteriorate the accuracy and quality of the workpiece being ground, which are difficult to be removed by subsequent polishing processes [19–21]. How to control and suppress the grinding marks is becoming a critical issue to optimise the grinding operation. Therefore, a theoretical model should be developed to describe the formation of surface patterns under various grinding conditions. It was found that the vibration caused by an unbalanced wheel is the primary source of grinding marks in ultra-precision grinding [22–24]. Chen et al. [25] analysed the influence of the micro-vibration of the grinding wheel on the surface quality of the workpiece generated in ultra-precision grinding and established a mathematical model describing the error of the surface profile of the workpiece caused by the vibration with a presumed simple sinusoidal signal. Kuriyagawa et al. [26] developed a 2D model to analyse the relationship between the grinding marks and grinding conditions. It was found that concentric circular patterns and spiral marks are involved in the nano-topography generation. The concentric circular patterns result from the revolution speed variation of the grinding wheel or workpiece. The spiral patterns are caused by the wheel unbalance, which is quite difficult to eliminate. In order to control and reduce the nano-topography caused by the grinding marks, Yoshihara et al. [27] developed a 2D model to describe the amplitudes of cross-sectional profile under different speed ratios between wheel rotation frequency and workpiece rotation frequency, and spatial frequency analyses were adopted to verify the simulation results. However, the surface topography of the workpiece is affected by many more factors. There is a lack of comprehensive study of the possible elements involved in the surface generation in ultra-precision grinding, and the surface generation mechanism is still not well understood.

In order to gain insight into the surface generation in ultra-precision grinding and the effect of grinding variables on the ground surface, the Taguchi method was firstly employed to evaluate the relative effect of the machining parameters, and then single-factor experiments were carried out to investigate the correlation among each grinding parameter on the surface generation. Hence, a theoretical model for predicting the regular spiral patterns was built and verified by experiments. Different mechanisms of material removal that contribute to surface generation were also investigated.

2 Experimental details

In ultra-precision grinding, the material is removed by a combination of the fast-rotating grinding wheel, a fine feed speed, very small depth of cut and slow spindle speed from the workpiece. The ground surface is generated by the continuous movement of the tool edge profile along the traverse direction (ignoring the abrasive grains). As shown in Fig. 1, a high-speed spinning grinding wheel (V_2) and the workpiece spindle speed V_1 together with a fine feed speed (V_f) under a tiny depth of cut (H) can produce path interference in adjacent passes of the wheel, which is responsible for the surface generation.

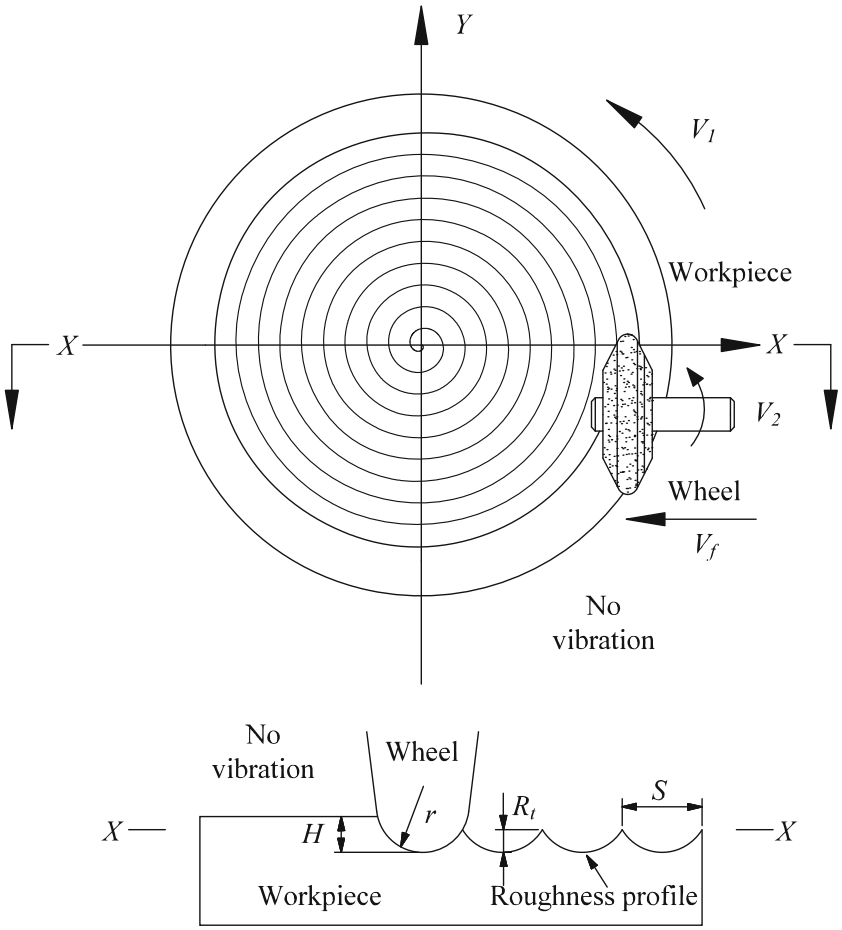

Fig. 1 Surface generation in ultra-precision grinding

Operational parameters can decide the radial locus of the grinding wheel to cut the workpiece and can influence the surface roughness and surface topographies of the workpiece. It is clear that the tool cutting parameters, wheel geometry and relative displacement between the tool and the workpiece have a significant influence on surface generation. The maximum peak-to-valley height of an ideal ground profile R_t can be calculated as [28]

$$R_t = r - \sqrt{r^2 - \frac{S^2}{4}} = r\left(1 - \sqrt{1 - \frac{S^2}{4r^2}}\right) \tag{1}$$

Due to $S << r$

$$R_t = \frac{S^2}{8r} = \frac{{V_f}^2}{8r{V_1}^2} \tag{2}$$

where r is the nose radius of the grinding wheel; S is the wheel traverse distance when the workpiece completes one revolution, which is in mm/rev; V_f is the tool feed speed in mm/min and V_1 is the rotational speed of the workpiece in r/min.

In the present study, ultra-precision grinding experiments were performed on a Moore Nanotech 450UPL ultra-precision grinding machine, which has two rotating spindles for the grinding wheel holder and the workpiece. The wheel holder is installed on a rotary b-axis, and the workpiece holder can be moved along the x-axis, as shown in Fig. 2. In the experiments, a resin bonded diamond wheel with a grain size number of 500 was used and RB-SiC was selected as the grinding material. The experimental conditions and material properties of RB-SiC are summarised in Tables 1 and 2, respectively.

The major error sources and uncertainties originate from the random nature of the grinding wheel. In order to minimise the disturbance of the random errors, the spindle rotational speed of the grinding wheel was kept stable at 40000 rpm in the Taguchi experiments and in the single-factor tests.

The Taguchi approach is an engineering optimization method which is used to evaluate the influence of process parameters or variables on process or product quality. It is able to optimise the machining parameters effectively with a minimum number of trials. To obtain a high performance in grinding RB-SiC, a combination of the grinding parameters was designed based on the Taguchi approach to evaluate the

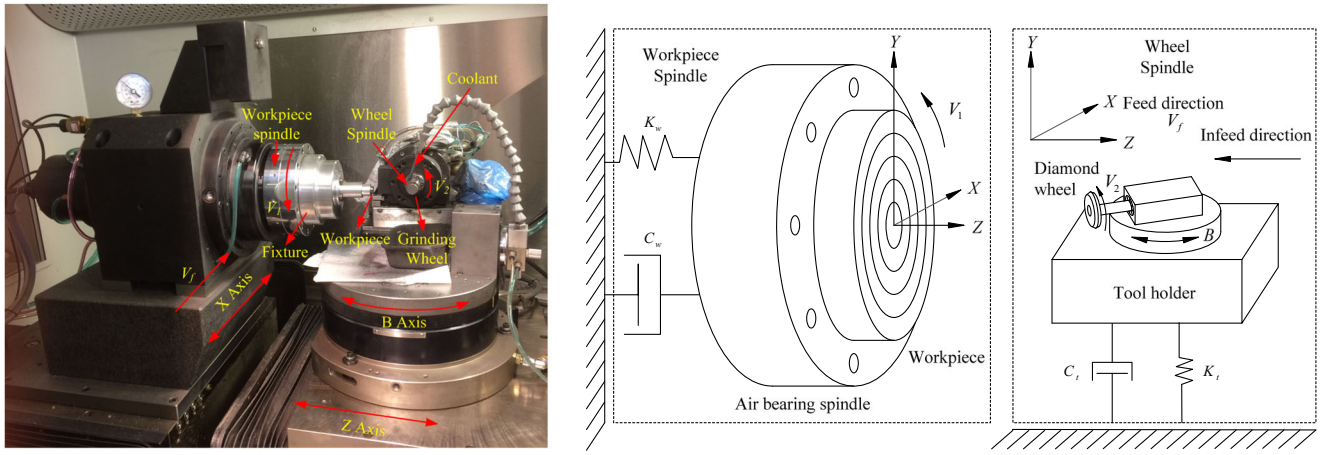

Fig. 2 Schematic diagram of the grinding machine

contribution of the process parameters (workpiece spindle rotational speed V_1, depth of cut H and feed speedV_f) with three levels on the arithmetical mean deviation of the profile (Ra). As shown in Table 3, the Taguchi method adopts the design of an orthogonal array, in which the three grinding factors are arranged in a L9 (3^3) orthogonal array. The grinding parameters were varied including the spindle speed of the workpiece (V_1) in the range 500 to 1500 rpm, the depth of cut (H) was varied from 5 to 15 μmand the feed speed (V_f) used was in the range of 5 to 15 mm/min. Finally, the experimental results were converted into a signal-to-noise (S/N) ratio which was used to measure surface quality.

3 Experimental results and theoretical analysis

3.1 Parametric analysis of surface generation

The measurement of the surface roughness of the workpiece was conducted using the non-contact Zygo Laser Interferometer Profiler System. The arithmetic roughness of the profile (Ra) is shown in Table 4. Figure 3 shows the value of the S/N ratios of three grinding parameters on the Ra value at different levels. In these experiments, the smaller-the-better optimisation criterion was adopted for the average S/N ratio and the larger value for the ratio infers better surface finish as shown in Table 5. It indicates that the feed speed (V_f) is a dominant variable for surface roughness followed by spindle speed of the workpiece (V_1). The depth of cut (H) has an insignificant effect on surface roughness. Figure 3 indicates that the optimal combination of grinding operation parameters is A3B2C1 (V_1 = 1500 rpm, H = 10 μm, V_f = 5 mm/min).

Figure 4 shows the surface topographies of the ground RB-SiC surfaces. It was found that the most significant feature of the machined surfaces is the spiral marks around the rotational centre of the workpiece, which does not correspond to that of the ideal surface as shown in Fig. 1, without micro-vibration. Furthermore, the number of spirals is equal to the ratio of the rotational speed of the grinding wheel V_2 to the spindle speed of workpiece V_1, e.g. the spirals in Fig. 4a–c, and the number of the spiral marks is equal to 80 (V_2/V_1 = 40,000/500 = 80) in one circle. The ratio space was much larger than the distance the tool travelled, and the shape of spiral marks varied as the grinding parameters were varied, indicating that tool vibration is involved in surface generation in ultra-precision grinding. It is indicated that the vibration of the grinding wheel at the tool rotational frequency has a dominant impact on the evolution of surface generation. It was observed that the spiral density

Table 1 Grinding wheel and grinding parameters

Grinding wheel	Resin bonded diamond wheel: 500-grit, diameter: 18 mm, thickness: 5 mm, nose radius: 0.5 mm, concentration 100%, structural number 7
Speed of the grinding wheel (V_2) (rpm)	40,000
Speed of the workpiece(V_1)(rpm)	500, 1000, 1500
Feed rate (V_f) (mm per min)	5, 10, 15
Depth of cut (μm)	5, 10, 15
Dresser and truer	Single diamond nib and aluminium oxide stick
Coolant	CLAIRSOL 330

Table 2 Material properties of RB-SiC

Workpiece	Reaction bonded SiC
Compressive strength (MPa)	2000
Young's modulus (H) (GPa)	410
Vickers hardness (H_v) (GPa)	2500
Fracture toughness (K_{IC})(MPa·m½)	4.0
Density (g/cm^3)	3.1
Dimension (length × width × height)	9 mm × 9 mm × 5 mm

Table 3 Taguchi experimental design

No.	Control factors	Levels		
		1	2	3
A	V_1 (rpm)	500	1000	1500
B	H (μm)	5	10	15
C	V_f (mm/min)	5	10	15

decreases with an increase of workpiece rotational speed (from $V_1 = 500$ to 1000 rpm) when the speed ratio was an integer, which is related to the fact that the number of spirals is equal to the ratio, as shown in Fig. 4a–f. However, when the ratio was not an integer ($V_2/V_1 = 40{,}000/1500 \approx 26.67$), the spiral density underwent a sharp increase, as shown in Fig. 4g–i. In this case, a phase shift (i.e. the fractional part of the ratio) generated an angle increment when the workpiece rotates one revolution, which indicates an accumulation of phase shift in the grinding cycles.

Based on the optimal result of the Taguchi experiments, a single-factor experiment was conducted to evaluate the effect of each machining parameter (i.e. workpiece rotational speed V_1, depth of cut H and feed speed V_f) on the surface quality (Table 6). The effect of the process parameters on the surface roughness is shown in Fig. 5. It was found that the surface roughness increased with increasing feed speed from 5 to 15 mm/min. The smaller feed speed resulted in the aggravation of the interference of the cutting profile of the wheel which leads to higher surface quality. The surface roughness decreased with increasing depth of cut from 5 to 10 μm. From 10 to 15 μm, the surface roughness slightly increased and the change in surface roughness was very tiny, which agrees well with the result of the Taguchi experiments. As the rotational speed of the workpiece increased, the surface roughness decreased, caused by the decrease of cross-feed distance (V_f/V_1). The cross-feed distance represents the distance that the grinding wheel moves towards the workpiece centre when the workpiece completes each revolution, which can increase neighbouring cutting profile interference resulting in a good surface finish. In Fig. 5d, for the same cross-feed distance, the average value of the surface roughness is used. With the increase of the cross-feed distance, the surface roughness increases. This shows that the cross-feed distance is also an important variable affecting the surface quality of the workpiece, which can reduce the scallop-height significantly so as to obtain a good surface finish.

Table 4 Experimental results for Ra

Experiment no.	Control factors			
	A	B	C	*Ra* (μm)
1	1	1	1	0.148
2	1	2	2	0.180
3	1	3	3	0.214
4	2	1	2	0.184
5	2	2	3	0.194
6	2	3	1	0.133
7	3	1	3	0.164
8	3	2	1	0.099
9	3	3	2	0.182

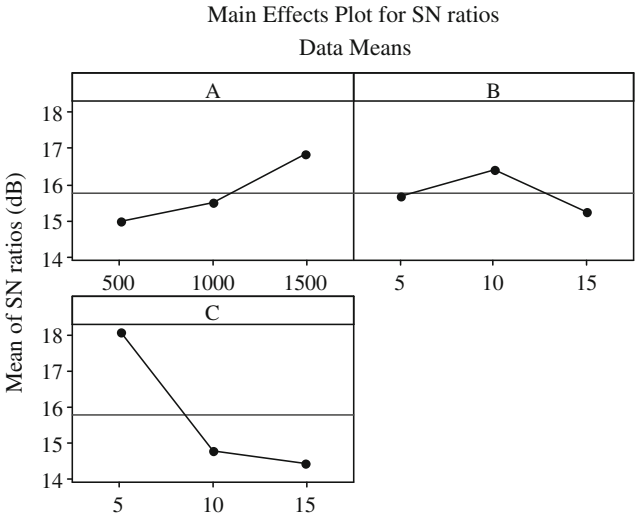

Fig. 3 *S/N* ratio graph for the surface roughness *Ra*

In order to investigate the effect of phase shift on surface generation in grinding, different phase shifts (0, 0.1…1.0) for different workpiece spindle speeds ($V_1 = 500$ rpm, $V_1 = 1000$ rpm and $V_1 = 1500$ rpm) were used. The rotational speed of the grinding wheel was increased starting at $V_2 = 39000$ rpm at 50-, 100- and 150-rpm intervals, respectively, until the two rotational speeds' ratio (V_2/V_1) was an integer again. Figure 6 shows the influence of phase shift on arithmetical surface roughness (S_a), it is interesting to note that all three curves embrace the similar tendency, as the phase shift increases from 0 to 0.1, and the surface quality improves significantly although the variation of three rotational speeds is very small. With the continuous increase of the phase shift to 0.6, the surface roughness was found to keep on improving. However, the surface quality became worse afterward with

Table 5 *S/N* ratio factor response for Ra

Technical parameters	Levels				
	1	2	3	Δ	Rank
A	14.96	15.49	16.86	1.90	2
B	15.67	16.41	15.24	1.17	3
C	18.07	14.80	14.45	3.62	1

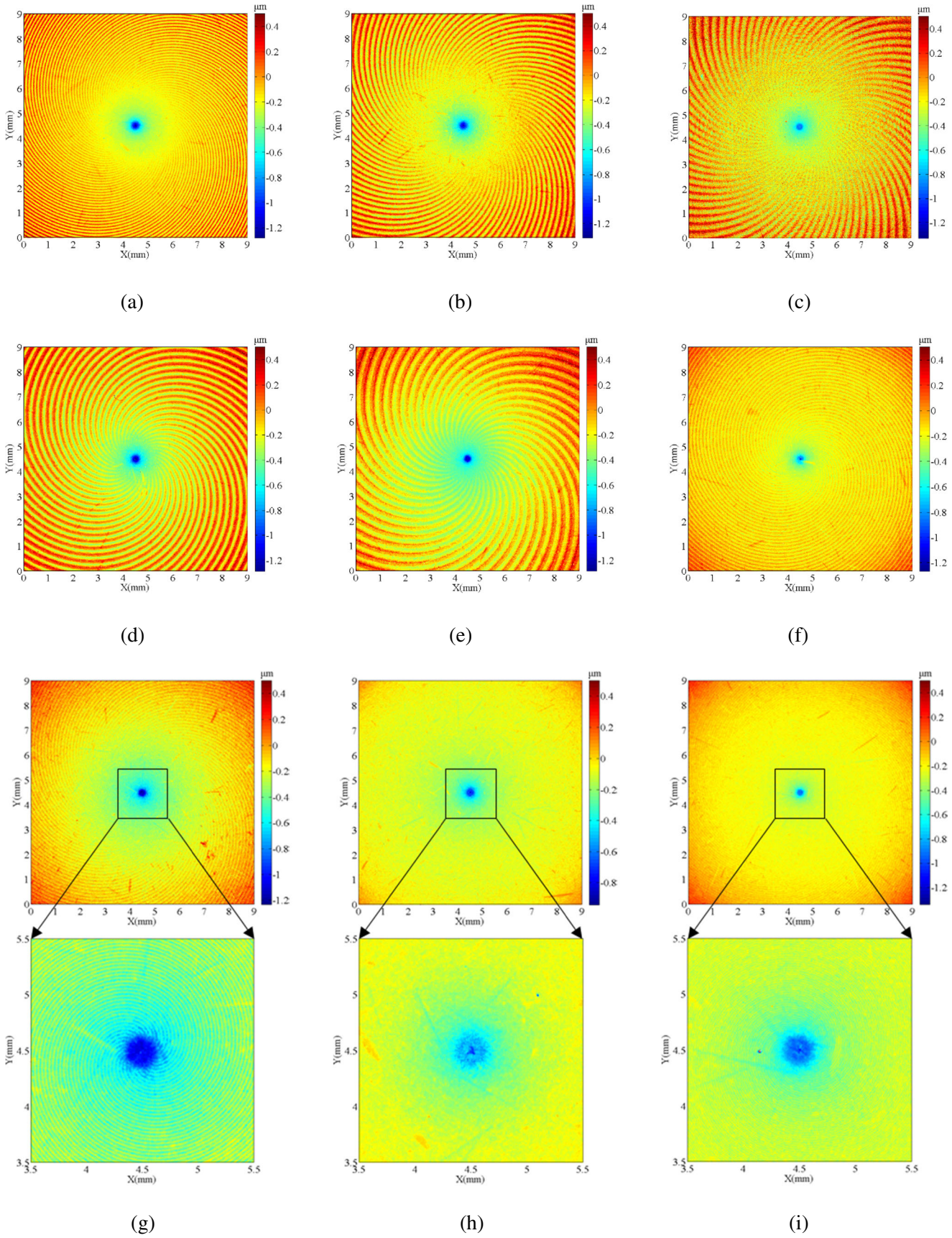

Fig. 4 Contour map of surface topography determined in the Taguchi experiment

Table 6 Single-factor experimental results

No.	V_1	H	V_f	V_f/V_1	Ra (μm)
1	1500	10	5	0.003	0.082
2	1500	10	10	0.007	0.133
3	1500	10	15	0.010	0.236
4	1500	5	5	0.003	0.078
5	1500	10	5	0.003	0.073
6	1500	15	5	0.003	0.080
7	500	10	5	0.010	0.176
8	1000	10	5	0.005	0.121
9	1500	10	5	0.003	0.070

an increase of the phase shift from 0.6 to 1.0. This suggests that the phase shift has a prominent effect on the surface finish of the ground surface. In order to obtain a better surface finish in grinding, the middle phase shift is preferable.

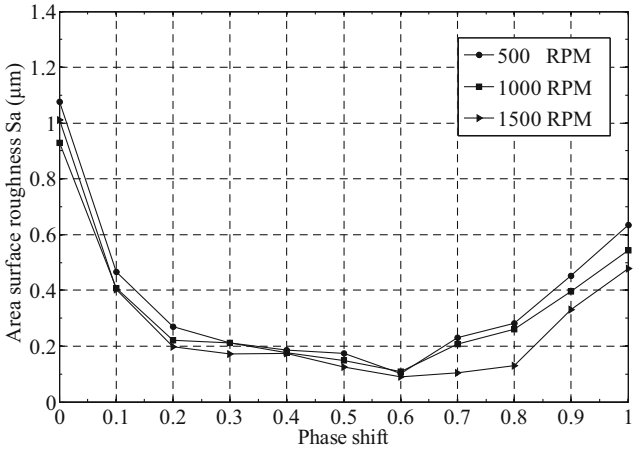

Fig. 6 Influence of phase shift on surface roughness

3.2 Theoretical analysis of the surface generation

A theoretical model was purposely built to analyse the surface generation in ultra-precision grinding. The spiral masks were found to have a significant effect on surface quality, which has a strong correlation with the ratio of the rotational frequency of the grinding wheel to the workpiece. Figure 7 shows the mechanism of the generation of the spiral masks in the grinding process. After the workpiece rotates one revolution, the cross-feed distance that the grinding wheel travels over the workpiece (direction of feed) is $S = V_f/V_1$. Under ideal conditions with an integer ratio, the spiral marks have the same rotational angle as the previous tool masks without a phase shift, which indicates the contour lines are straight lines instead of spirals. For a non-integer ratio, the fractional part of the ratio generates an increment Φ in phase shift when the workpiece rotates one revolution, which is responsible for the evolution of the spiral masks. In actual grinding operation, the phase shift always exists in the entire process due to the fluctuation of rotational frequency of the grinding wheel or the workpiece. The locus of the grinding wheel is shown in Fig. 8.

The workpiece rotates an angle $\Delta\theta$ when the grinding wheel completes one revolution Δt, which can be expressed as

$$\Delta t = \frac{60}{V_2} \tag{3}$$

$$\Delta\theta = \frac{2\pi V_1}{V_2} \tag{4}$$

In the grinding, the number of spiral marks is equal to the integer part of the rotating ratio of the wheel and workpiece. The phase shift $\mathbf{\Phi}$ represents the fractional part of the rotating ratio, which can be calculated as

$$\mathbf{\Phi} = 2\pi\left[\frac{V_2}{V_1} - \mathrm{int}\left(\frac{V_2}{V_1}\right)\right] \tag{5}$$

In discrete form, the harmonic motion of the grinding wheel can be expressed as

$$Z(t_j) = A\sin\left(\frac{2\pi f_2 j\Delta\theta}{\omega_2} + \varphi\right) \quad j = 0, 1, 2, \ldots, N_t \tag{6}$$

$$N_t = \frac{2\pi}{\omega_1\Delta t}\cdot\frac{R_0 V_1}{V_f}$$

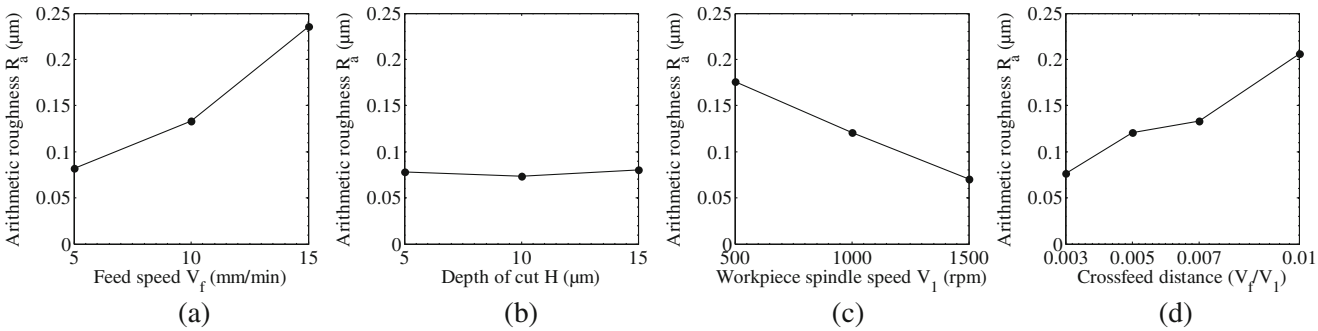

Fig. 5 Effect of processing parameters on surface roughness in the grinding of RB-SiC

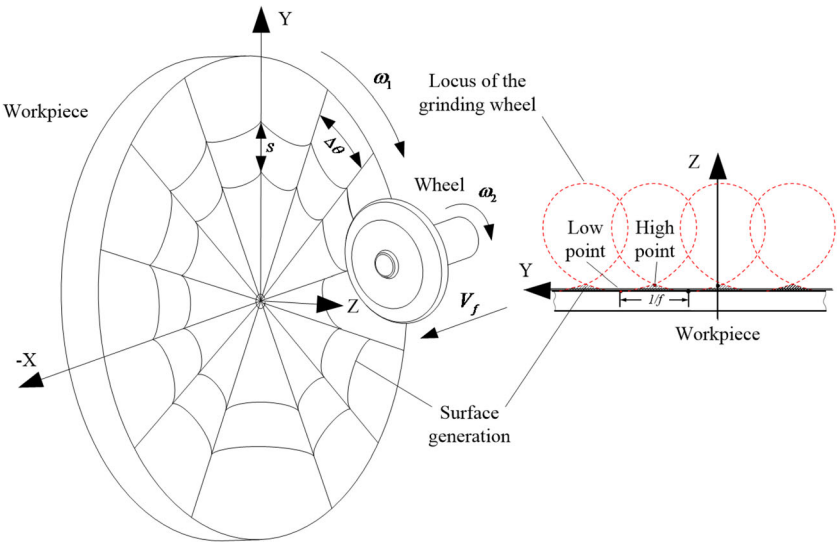

Fig. 7 Spiral marks generated by the wheel with micro-vibration

where f_2 is the rotational frequency of the grinding wheel and A is the vibration amplitude.

$$\theta(i,k) = k\Delta\theta + 2\pi(i-1), i = 1,2,\ldots,N_w$$
$$N_w = \frac{R_0 V_1}{V_f}, k = 0,1,2,\ldots,N_s \quad N_s = \frac{2\pi}{\omega_1 \Delta t} \tag{7}$$

$$R(i,k) = R_0 - [k + (i-1)N_s]\Delta r \quad \Delta r = \frac{V_f}{V_2} \tag{8}$$

In the $X-Y$ plane, the locus of the grinding wheel is given by

$$X(i,k) = R(i,k)\cos[k\Delta\theta + 2\pi(i-1)] \tag{9}$$
$$Y(i,k) = R(i,k)\sin[k\Delta\theta + 2\pi(i-1)] \tag{10}$$

In order to investigate the relationship between the phase shift and the spiral geometry, a single spiral simulation was conducted, during which the deepest point of interaction between the

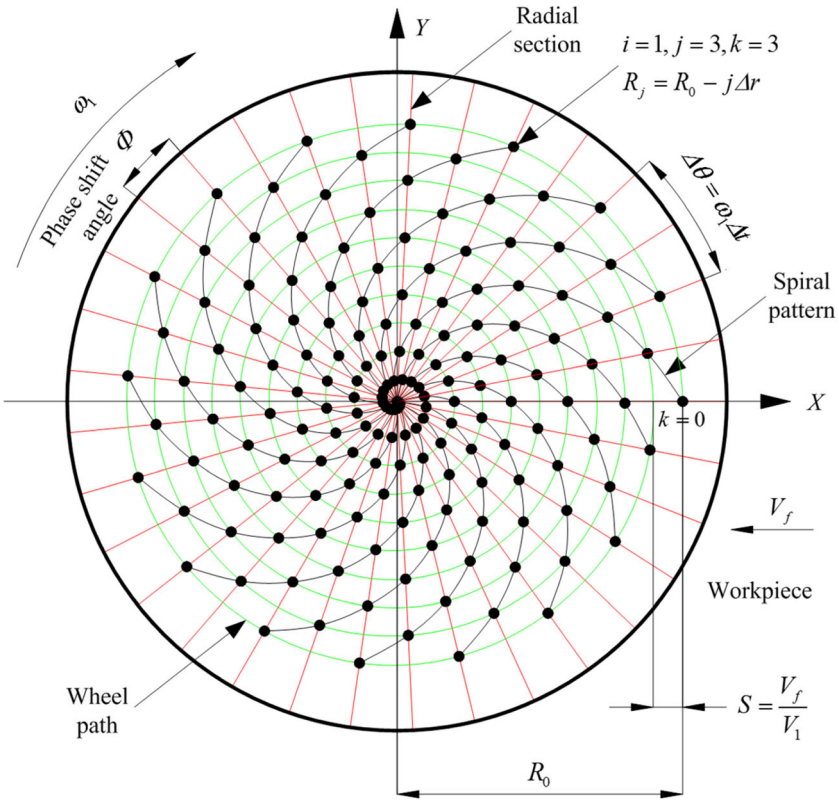

Fig. 8 Locus of the lowest point for the grinding wheel

wheel and the workpiece was considered. A simulation tool has been developed to implement model analysis of the surface generation in ultra-precision grinding by the MATLAB programming software. In ultra-precision grinding, the grinding wheel cannot maintain complete invariability; instead, there is a small revolution error which means that a phase shift is inevitable. It was found that the actual rotational speed of the wheel is about 20 rpm larger than the preset value. Figure 9 shows simulated results of the single spiral generation for different phase shifts (0, 0.1…1.0) through changing the rotational speed of the grinding wheel from 39,000 to 40,500 rpm at 150-rpm intervals. It was found that with the increase of the phase shift (0–0.4), the cycles of spiral increased. When the phase shift was equal to 0.4, 0.5 and 0.6, the number of cycles remained equal, but after that, the number decreased. At the same time, the direction of rotation of spiral changed from anticlockwise to clockwise from the edge area to the centre area. Figure 10 shows the maps of grinding marks measured with the Zygo laser interferometric profiler. Due to the dense spiral marks along with the accumulation of the phase shift, the small area (length × width = 2 mm × 2 mm) in the centre region of the workpiece was selected to make the spiral clearer to observe when the phase shift changed from 0.2 to 0.8, as shown in Fig. 10c–i. It can be observed that the test results agreed well with simulated spiral marks shown in Fig. 9.

The modelling of the surface pattern shown previously gives the interaction between the wheel and the workpiece without considering the variations of the feed rate. In fact, in the spark out stage, the feed speed was decreased gradually from the set value to 0 and the tool was then withdrawn and stopped. As a result, the area near the centre was different from the rest of the ground surface.

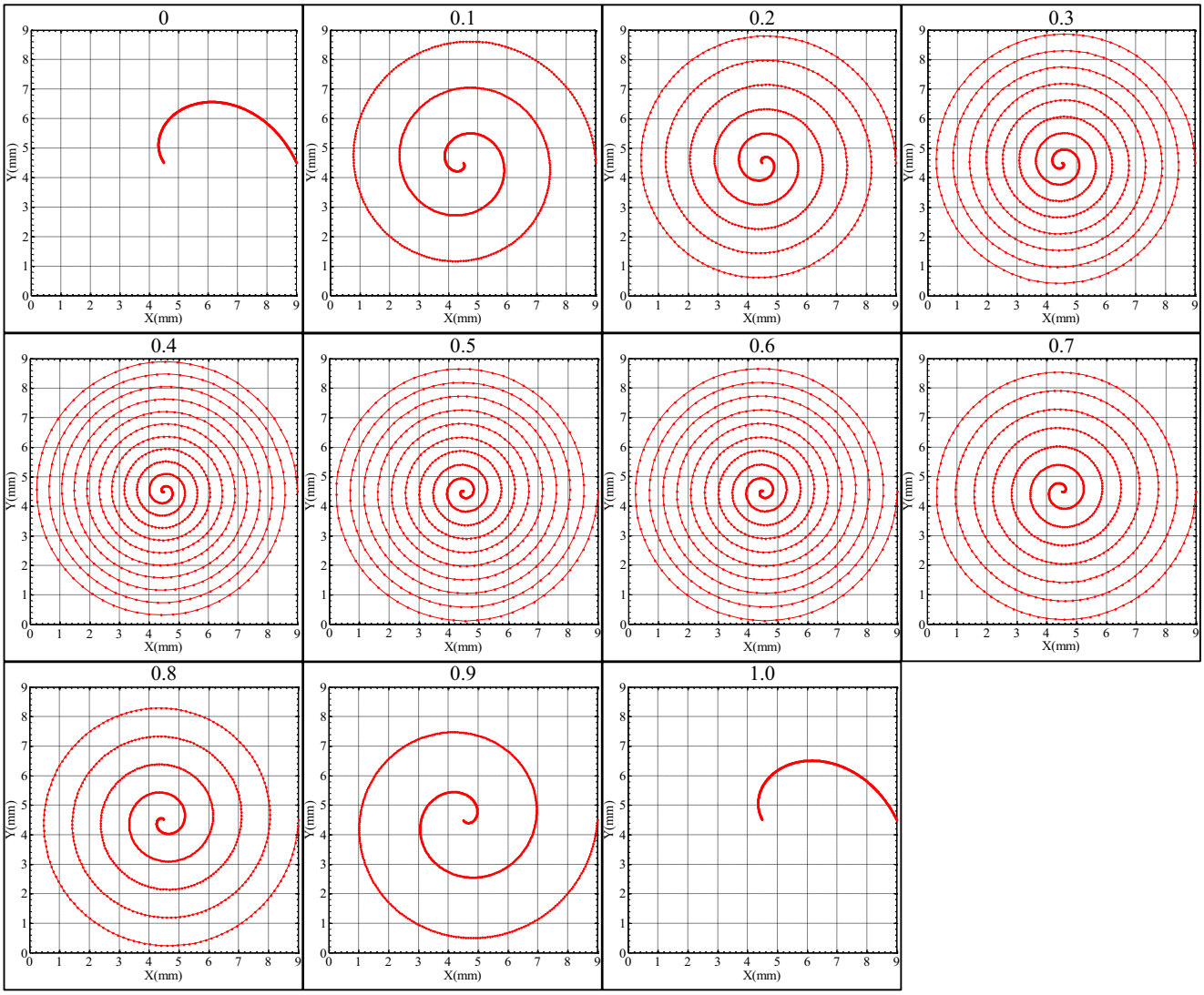

Fig. 9 Simulation of single spiral generation (phase shift 0, 0.1…1.0), rotational speed of the grinding wheel: 39000–40,500 rpm, feed rate: 10 mm/min, rotational speed of the workpiece 1500 rpm

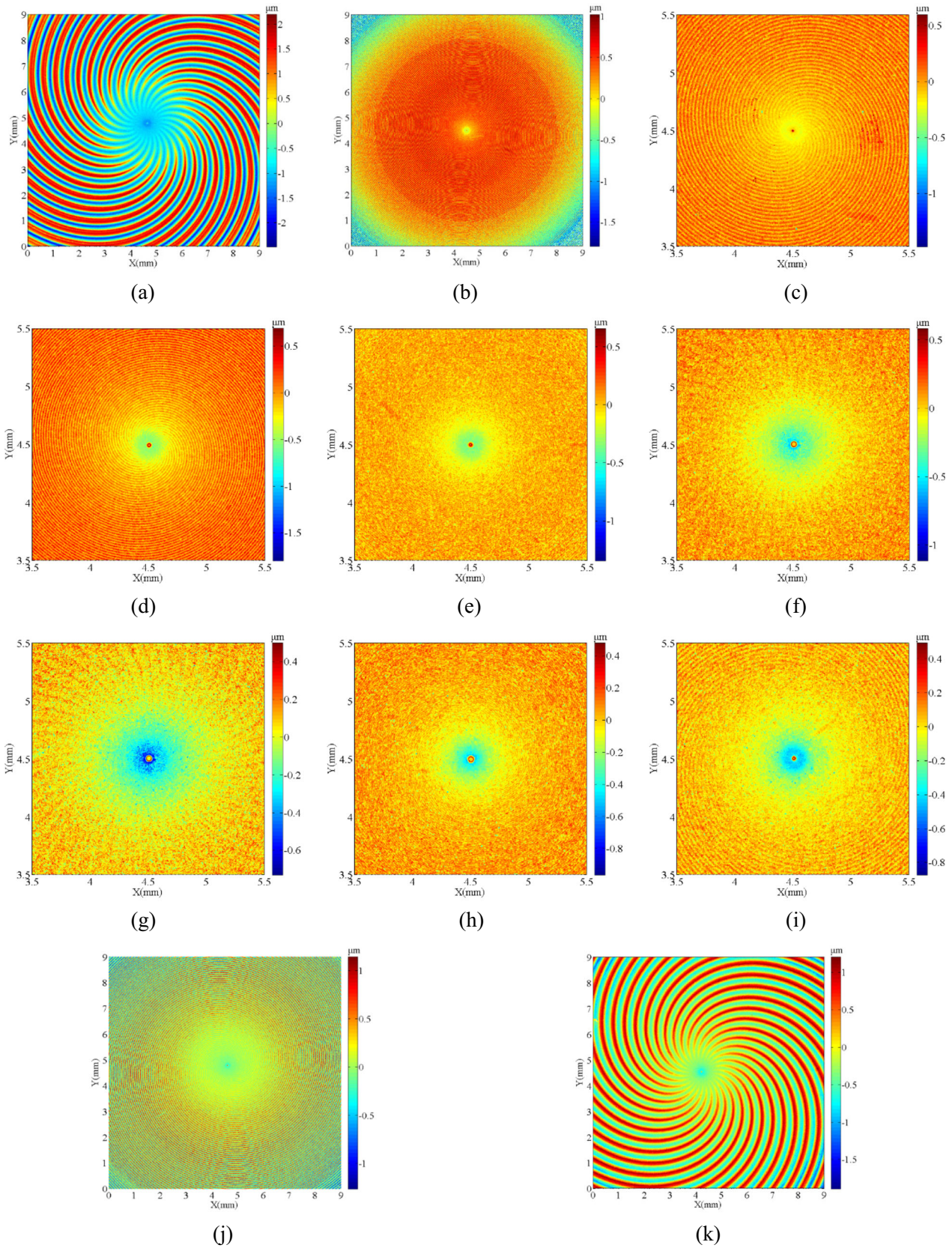

Fig. 10 Measured surface topography for different phase shifts (0, 0.1…1.0). The wheel speed V_2 from 39,000 to 40,500 rpm at 150-rpm intervals (V_1 = 1500 rpm, V_f = 10 mm/min, H = 10 μm)

The position of the grinding wheel with respect to the workpiece can be amended as

$$X_p(i,k) = \left(R_e - V_f \frac{\Delta\theta}{\omega_1} - a\frac{\Delta\theta^2}{2{\omega_1}^2}\right)\cos[k\Delta\theta + 2\pi(i-1)] \quad (11)$$

$$Y_p(i,k) = \left(R_e - V_f \frac{\Delta\theta}{\omega_1} - a\frac{\Delta\theta^2}{2{\omega_1}^2}\right)\sin[k\Delta\theta + 2\pi(i-1)] \quad (12)$$

where R_e is the distance between the starting position of the wheel slowed for feed speed on the workpiece and the centre of rotation of the workpiece.

$a < 0$ is the acceleration of feed speed near the central area.

With the development of wheel wear under micro-vibration, more than one high point on the wheel surface may have the opportunity to make contact with the workpiece [29]. Figure 11 shows two high points on the grinding wheel interacting with the workpiece, and thus, the number of waviness marks is doubled.

In order to calculate surface topography in each radial section, the shape of the wheel should be determined firstly. The grinding wheel profile having the wheel radius (R_w) and a nose radius (r_w) was modelled as an ellipsoid as shown in Fig. 12, which can be expressed as

$$\left(\frac{x}{R_w}\right)^2 + \left(\frac{y}{R_y}\right)^2 + \left(\frac{z}{R_w}\right)^2 = 1 \quad (13)$$

Where R_w and R_y are the semi-major axis and the semi-minor axis of the ellipse, respectively.

In order to calculate (R_y), the radius of curvature (r_w') in the $Z-Y$ section is derived as

$$r_w' = \frac{1}{\rho} = \frac{\left[1 + \left(\frac{\partial z}{\partial y}\right)^2\right]^{\frac{3}{2}}}{\left|\frac{\partial^2 z}{\partial y^2}\right|} \quad (14)$$

$$r_w' = \frac{1}{\rho} = \frac{\left[1 + \frac{y^2 {R_w}^2}{{R_y}^4}\left(1 - \frac{y^2}{{R_y}^2}\right)^{-1}\right]^{\frac{3}{2}}}{\left|\frac{R_w}{{R_y}^2}\left(1 - \frac{y^2}{{R_y}^2}\right)^{-\frac{1}{2}}\left(1 - \frac{y}{{R_y}^2}\left(1 - \frac{y^2}{{R_y}^2}\right)^{-1}\right)\right|} \quad (15)$$

At the lowest contact point ($y = 0$), the tool nose radius of the wheel is given as

$$\frac{1}{\rho} = \frac{{R_y}^2}{R_w} = r_w \quad (16)$$

$$R_y = \sqrt{R_w r_w} \quad (17)$$

The final ellipsoid equation is denoted as

$$\frac{x^2 + z^2}{{R_w}^2} + \frac{y^2}{R_w r_w} = 1 \quad (18)$$

To drive the intersection of a neighbouring cutting profile, cross section of the grinding wheel in the Z-Y plane can be expressed as

$$z = -\sqrt{{R_w}^2 - \frac{R_w y^2}{r_w}} \quad (19)$$

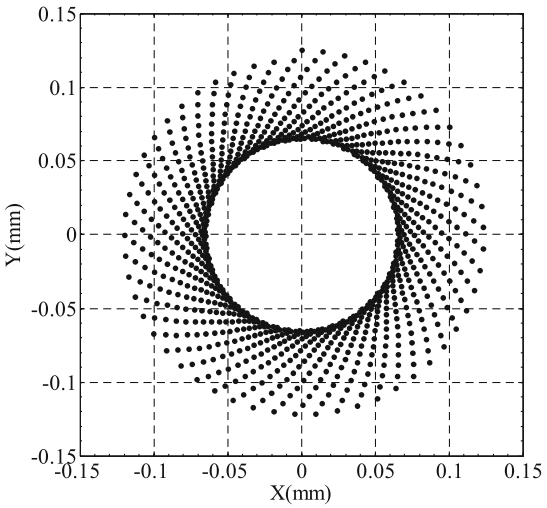

(a)

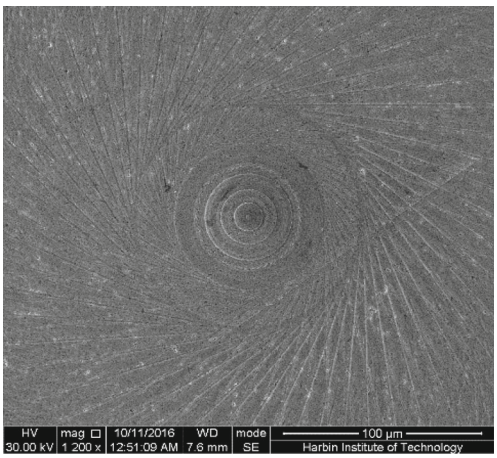

(b)

Fig. 11 The centre area **a** simulated surface pattern, **b** SEM map of ground surface ($V_1 = 1500$ rpm, $V_2 = 40{,}000$ rpm, $V_f = 10$ mm/min, $H = 10$ μm)

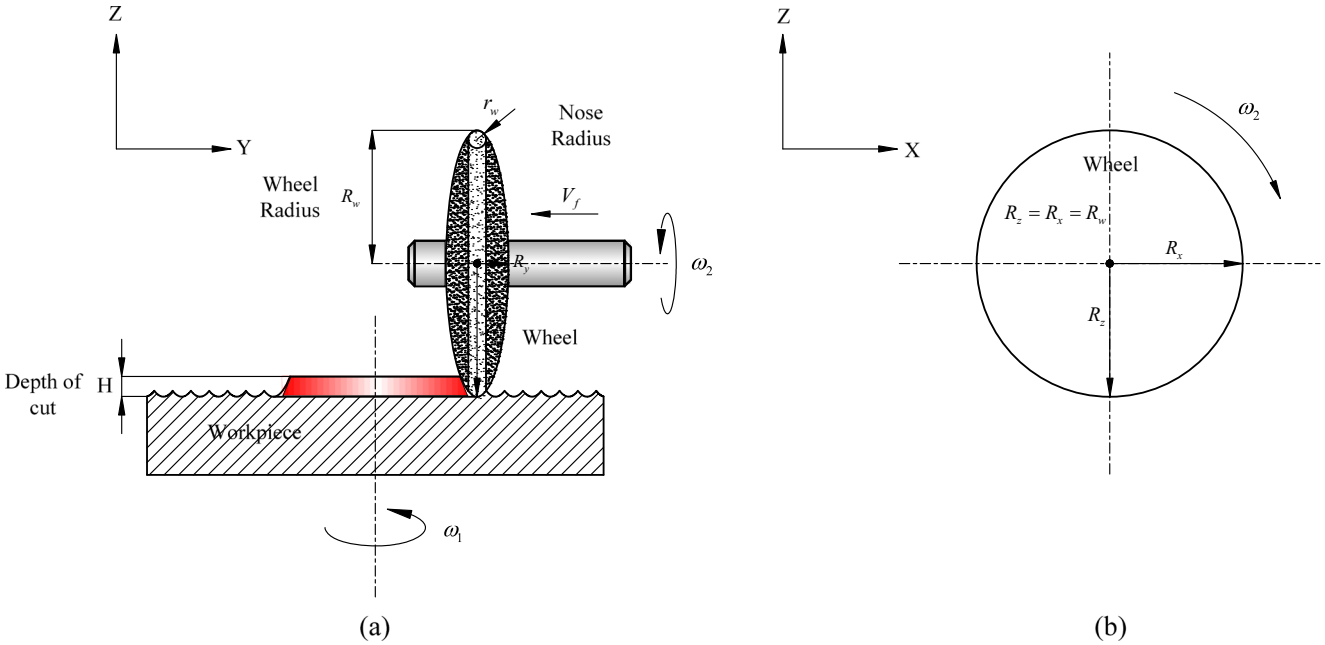

Fig. 12 Graphical illustration of the grinding wheel. **a** Front view of the wheel. **b** Side view of the wheel

In discrete form:

$$Z_{i,k}(r_{i,k}) = -\sqrt{{R_w}^2 - \frac{R_w\left[r_{i,k} - (\mathrm{i}-1)S\right]^2}{r_w}} \tag{20}$$

The cutting profile for the ith and $i+1$st at the kth radial section can be expressed as

$$Z_c(r_{i,k}) = A\sin\left\{\frac{2\pi f_2[k+(i-1)N_s]\Delta\theta}{\omega_2} + (i-1)\Phi\right\} + Z_{i,k}(r_{i,k}) \tag{21}$$

$$Z_c(r_{i+1,k}) = A\sin\left[\frac{2\pi f_2(k+iN_s)\Delta\theta}{\omega_2} + i\,\Phi\right] + Z_{i+1,k}(r_{i+1,k}) \tag{22}$$

For the intersection of the ith and $i+1$st cutting tool profile at the kth radial section, $Z(R_{i,k}) = Z(R_{i+1,k})$ and $r_{i,k} = r_{i+1,k}$. Thus, the height $Z_{i,i+1,k}$ of the intersection is determined as

$$Z_{i,i+1,k} = \frac{r_w}{2}(A_i + A_{i+1}) - \sqrt{\frac{r_w(A_i + A_{i+1})^2 + r_w(A_{i+1} - A_i)^2 + R_wS^2}{4r} - \frac{R_wS^2(A_i - {R_w}^2)}{r_w(A_{i+1} - A_i)^2 + R_wS^2}} \tag{23}$$

$$r_{i,i+1,k} = -\frac{2r_wZ_{i,i+1,k}(A_{i+1} - A_i) + r_w\left({A_{i+1}}^2 - {A_i}^2\right) + R_wS^2(1-2i)}{2R_wS} \tag{24}$$

where $A_i = A\sin\left\{\frac{2\pi f_2[k+(i-1)N_s]\Delta\theta}{\omega_2} + (i-1)\Phi\right\}$, $A_{i+1} = A\sin\left[\frac{2\pi f_2(k+iN_s)\Delta\theta}{\omega_2} + i\,\Phi\right]$

According to Eqs. 11–24, all ground surface topographies in different radial sections can be calculated. Figure 13 shows that the model agree with the experiments in terms of *Sa* under different phase shifts ($V_1 = 1500$rpm) in the grinding of RB-SiC, in which the measured and calculated area are $X_L = Y_L =$ 1 mm, and the centre of the selected area $X_O = Y_O = 3$ mmwith respect to the centre of workpiece.

Material properties play an important role in the process of chip formation and surface generation, especially for ceramics materials, which differ considerably from metals in regard to grinding [30]. In order to study the different mechanisms of surface generation for different types of material, RB-SiC, mould steel (S136) and tungsten carbide (WC) were chosen for the grinding experiments. As shown in Fig. 14, spiral marks were observed on the ground surfaces of the three kinds of material; for steel and WC, the spirals were clearer to observe than for RB-SiC, which resulted from more fracture areas in comparison with

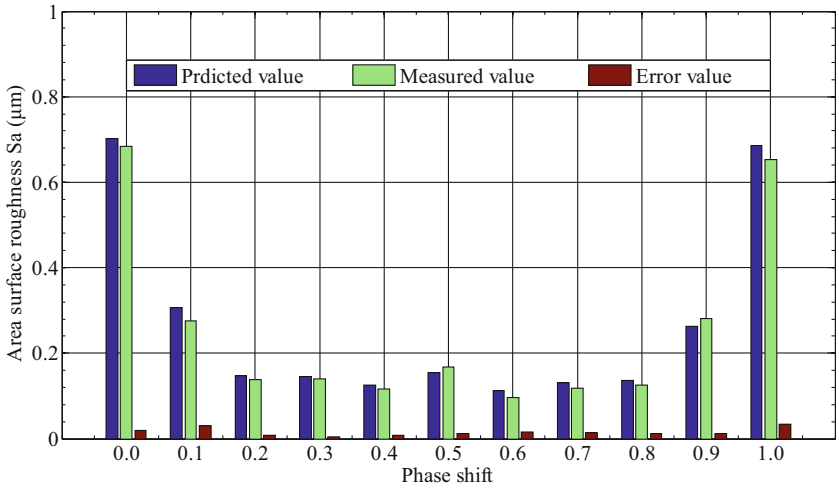

Fig. 13 Comparison diagram between predicted and measured area surface roughness

steel and WC. The machined surfaces contain micro-grooves produced by the micro-cutting of the grinding wheel, especially for steel and WC, which can be more clearly seen. For steel, the surface is generated by plastic flow, especially in the interaction between neighbouring cutting grooves, in which the later pass of the wheel extrudes the material aside. However, the machined surfaces for WC and RB-SiC were found to be more complex and contain micro-fracture regions, pits and ductile areas. It was found that even some smooth regions are covered with smeared particles and fine debris, where the removed material was trapped between the wheel and workpiece in the machining region. A few pits were observed on the machining surfaces of WC and RB-SiC. This indicated that considerable differences exist in the machining of brittle materials and ductile metals, as different modes of material removal are involved in the surface generation. It is interesting to note that the Spanzipfel effect was found in the grinding of the three kinds of materials, whereby a small portion of the materials was not removed by the cutting tool, but instead was left on the ground surface. The Spanzipfel effect is related to the minimum undeformed chip thickness, below which the chip cannot be formed [31, 32]. For steel, the Spanzipfel effect is more obvious than for WC and RB-SiC.

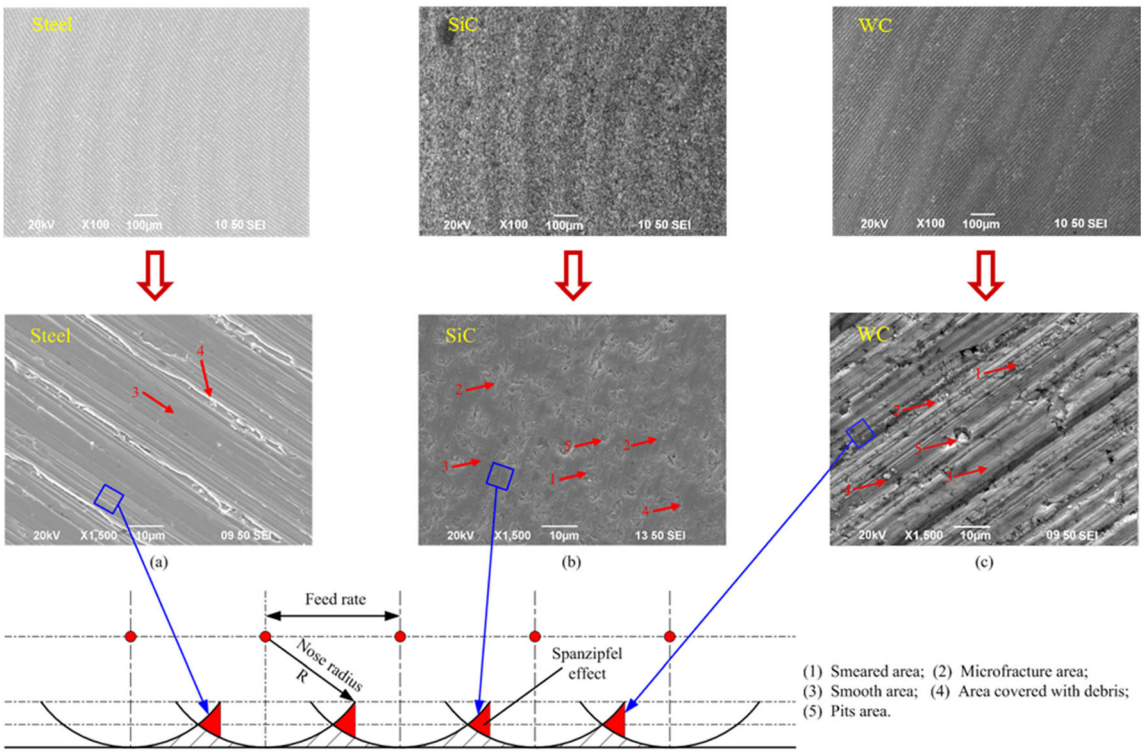

Fig. 14 SEM micro-graphs of ground surface for **a** steel, **b** RB-SiC and **c** WC ($V_1 = 1500$ rpm, $V_2 = 40{,}000$ rpm, $V_f = 10$ mm/min, $H = 10$ μm). Arrows point at five typical areas: (1) smeared areas, (2) micro-fracture areas, (3) smooth areas, (4) area covered with debris and (5) pit areas

4 Conclusions

Surface generation in ultra-precision grinding was systemically investigated both experimentally and theoretically. The ground surface quality was found to be primarily influenced by feed rate, workpiece spindle speed, synchronous vibration of the grinding wheel and phase shift. The optimal combination of the process parameters includes a small cross-feed distance and a finer feed rate as well as a medium phase shift. These factors can determine the trajectory of the grinding wheel and result in different surface topographies. A single spiral model was developed to reveal the evolution of spiral marks. It was found that the medium phase shift can result in dense spirals. The approximate straight-line pattern around one circle is caused by the gradual decrease of the feed speed near the end of the grinding operation. The surface generation in the grinding involves many mechanisms, such as spiral marks, Spanzipfel effect and phase shift. The Spanzipfel effect was found in the grinding of both ductile and brittle materials.

Funding information The work was supported by a PhD studentship (project account code: RU3K) from The Hong Kong Polytechnic University. This research work was also supported by the State Key Basic Research and Development Program, China (973 program, Grant No. 2011CB 013202), and Guangdong Provincial Department of Science and Technology, Guangdong, P.R. China, for The Introduction of Innovative R&D Team Program of Guangdong Province (project no.: 201001G0104781202).

References

1. Agarwal S, Rao PV (2012) Predictive modeling of undeformed chip thickness in ceramic grinding. Int J Mach Tools Manuf 56: 59–68
2. Beaucamp A, Simon P, Charlton P, King C, Matsubara A, Wegener K (2017) Brittle-ductile transition in shape adaptive grinding (SAG) of SiC aspheric optics. Int J Mach Tools Manuf 115:29–37
3. Jahanmir S, Ramulu M, Koshy P (1999) Machining of ceramics and composites. Marcel Dekker, New York
4. Zhang QL, To S, Zhao QL, Guo B, Zhang GQ (2015) Impact of material microstructure and diamond grit wear on surface finish in micro-grinding of RB-SiC/Si and WC/Co carbides. Int J Refract Met Hard Mater 51:258–263
5. Agarwal S, Rao PV (2010) Grinding characteristics, material removal and damage formation mechanisms in high removal rate grinding of silicon carbide. Int J Mach Tools Manuf 50:1077–1087
6. Yin L, Huang H (2008) Brittle materials in nano-abrasive fabrication of optical mirrorsurfaces. Precis Eng 32:336–341
7. Zhang B, Zheng XL, Tokura H, Yoshikawa M (2003) Grinding induced damage in ceramics. J Mater Process Technol 132(1–3): 353–364
8. Lee SC, Ren N (1996) Behavior of elastic-plastic rough surface contacts as affected by surface topography, load, and material hardness. Tribol Trans 39(1):67–74
9. Stark GA, Moon KS (1999) Modeling surface texture in the peripheral milling process using neural network, spline, and fractal methods with evidence of chaos. ASME J Manuf Sci Eng 121(2): 251–256
10. Huang H, Yin L, Zhou LB (2003) High speed grinding of silicon nitride with resin bond diamond wheels. J Mater Process Technol 141(3):329–336
11. Zhang QL, To S, Zhao QL, Guo B (2016) Surface generation mechanism of WC/Co and RB-SiC/Si composites under high spindle speed grinding (HSSG). Int J Refract Met Hard Mater 56:123–131
12. Kwak J (2005) Application of Taguchi and response surface methodologies for geometric error in surface grinding process. Int J Mach Tools Manuf 45(3):327–334
13. AllorRL, WhalenTJ, BaerJR, KumarKV (1993)Machining of silicon nitride: experimental determination of process/property relationships Proceedings of International Conference on Machining Adv Mater223–234
14. Oliveira JFG, Botteneand AC, França TV (2001) A novel dressing technique for texturing of ground surfaces. Annals of the CIRP—Manufacturing Technology 59:361–364
15. Ohbuchi Y, Obikawa T (2006) Surface generation model in grinding with effect of grain shape and cutting speed. JSME Int J Ser C Mech Syst Mach Elem Manuf 49(1):114–120
16. Agarwal S, Rao PV (2005) A new surface roughness prediction model for ceramic grinding. Proc Inst Mech Eng B J Eng Manuf 219(11):811–819
17. Warnecke G, Zitt U (1998) Kinematic simulation for analyzing and predicting high-performance grinding processes. Ann CIRP 47(1): 265–270
18. Cao YL, Guan JY, Li B, Chen XL, Yang JG, Gan CB (2013) Modeling and simulation of grinding surface topography considering wheel vibration. Int J Adv Manuf Technol 66(5):937–945
19. Jiang XH, Guo MX, Li BZ (2018) Active control of high-frequency tool-workpiece vibration in micro-grinding. Int J Adv Manuf Technol 94(1):1429–1439
20. Yan Y, Xu J, Wiercigroch M (2016) Regenerative chatter in self-interrupted plunge grinding. Meccanica 51(12):3185–3202
21. Hassui A, Diniz AE (2003) Correlating surface roughness and vibration on plunge cylindrical grinding of steel. Int J Mach Tools Manuf 43(8):855–862
22. Yoshihara N, Kuriyagawa T, Syoji K (2003) Formation of vertical striped pattern on the ground surface in high-reciprocation profile grinding (in Japanese). Journal of the Japan Society for Precision Engineering 67(8):1316–1320
23. Cao HR, Dörgeloh T, Riemer O, Brinksmeier E (2017) Adaptive separation of unbalance vibration in air bearing spindles. Procedia CIRP 62:357–362
24. Marinescu I, Rowe W, Dimitrov B, Ohmori H (2013) Tribology of abrasive machining processes, 2nd edn. Elsevier, Amsterdam
25. Chen JB, Fang QH, Li P (2015) Effect of grinding wheel spindle vibration on surface roughness and subsurface damage in brittle material grinding. Int J Mach Tools Manuf 91:12–23
26. Kuriyagawa T, Yoshihara N, Saeki M, Syoji K (2003) Nanotopography characterization of axisymmetric aspherical ground surfaces. Key Eng Mater 238-239:125–130
27. Yoshihara N, Yan JW, Kuriyagawa T (2008) Control of nanotopography on an axisymmetric ground surface. Key Eng Mater 389-390:96–101
28. Whitehouse DJ (1994) Handbook of surface metrology. Institute of Physics Pub, Bristol

29. Gill R (1986) An investigation into the effect of the ratio of grinding wheel speed to workpiece speed in the centreless grinding process. In: Coventry. Lanchester) Polytechnic, PhD thesis
30. Horvath M, Kundrak J, Mamalis A, Gyani K (2002) On the precision grinding of advanced ceramics. Int J Adv Manuf Technol 20(4):255–258
31. Pandit SM, Sathyanarayanan G (1984) Data-dependent systems approach to surface generation in grinding. ASME J Eng Ind 106(3):205–212
32. Pandit SM, Revach SS (1981) A data dependent systems approach to dynamics of surface generation in turning. ASME J Eng Ind 103(4):437–445